

Fiber Orientation Angle Effects in Machining of Unidirectional CFRP Laminated Composites

V. Madhavan^{1,3}, G. Lipczynski², B. Lane¹, and E. Whintont¹

¹Intelligent Systems Division
National Institute of Standards and Technology
Gaithersburg, Maryland, USA

²Boeing Research & Technology
The Boeing Company, Huntington Beach, California, USA

³Department of Industrial & Manufacturing Eng.
Wichita State University
Wichita, Kansas, USA

ABSTRACT

Experiments were carried out at the National Institute of Standards and Technology, in collaboration with The Boeing Company, to obtain force and temperature data as a function of feed, speed, and fiber orientation angle (FOA), for validation of finite element simulation of composite machining. The outer diameter of disks of unidirectional carbon fiber reinforced plastic (CFRP) laminates were cut orthogonally. Tabs were machined into the outer diameter (OD) to cause cutting to begin at a FOA of 0° and end at a FOA of 90°. Cutting forces were measured using a dynamometer and the chip morphology was recorded using a high speed camera. It was observed that the variation of cutting force with FOA depended on the feed. For large feed, the cutting force increases with FOA until an angle of 90°, whereas for low feed the cutting force decreases beyond 65°. The chip morphology also changes with FOA and feed. Significant tool flank wear is noted even in these short duration experiments, which causes the thrust and cutting forces to increase significantly for FOA from 0° to 60°. For 65° to 80° FOA, force signals change cyclically. A small spike in the cutting force seems to be correlated with fibers being pulled out in clumps, and is followed by lower forces in subsequent revolutions while the pitted surface is machined.

KEYWORDS

Carbon fiber reinforced plastic, composites machining, fiber orientation angle, tool wear, high speed videography

INTRODUCTION

Machining of composites, for example, the drilling of holes and routing of edges, is of high importance to the aviation industry. Damage of the machined surface and tool wear are among the primary concerns. Damage in the form of delamination across plies, surface pitting, etc., occurs due to extreme differences in the strength and ductility of the matrix and the reinforcing fibers. The high forces required for cutting through the fibers and the variation of forces with fiber angle can cause the matrix to debond from the fiber and to delaminate across plies. The force required and the damage beneath the machined surface are highly

dependent on the sharpness of the cutting edge of the tool, as many finite element analysis results have shown [1]. However, the effect of the edge radius on cutting mechanisms has been experimentally studied only to a very limited extent. Tool wear leads to blunting of the cutting edge and thereby affects the cutting forces, chip morphology, temperature, and damage. To reduce the effect of tool wear during the time it takes the cutting process to stabilize, the edges of most of the cutting tools used were prepared with a chamfer of about 0.015 mm. Experiments have been carried out to study changes in the cutting process when the feed changes from a low value to a value that is much larger than the edge radius.

Disclaimer: No approval or endorsement of any commercial product by the National Institute of Standards and Technology is intended or implied. Certain commercial equipment, instruments, or materials are identified in this report in order to facilitate understanding and verification of relevant characteristics. Such identification does not imply recommendation or endorsement by the National Institute of Standards and Technology, nor does it imply that the materials or equipment identified are necessarily the best available for the purpose. This publication was prepared by United States Government employees as part of their official duties and is, therefore, a work of the U.S. Government and not subject to copyright.

In all of the work to date on the machining of unidirectional composites, the effect of fiber orientation angle has been studied by orthogonal cutting in a planing-type configuration, carrying out experiments at discrete pre-set fiber orientation angles (FOAs). Orthogonal turning of disks presents a method to sample a continuum of FOAs, allowing detailed study of the variation in process outputs with FOA. Previous studies of the cutting of composites (beginning with Koplev [2]) have shown that the friction at the chip tool interface is negligible and that the cutting speed does not significantly affect the process. These, and the additional fact that the chips are mostly powdery, justify treatment of the cutting of an increment of the circumference of a disk at a particular FOA as a valid representation of cutting for longer durations at that FOA. The instantaneous data would be independent of any effect from the cutting of increments immediately before and after, that occur at different FOAs, provided the disk diameter and the bandwidth of the measuring instruments are suitably high.

Another advantage of studying orthogonal cutting of disks is its similarity to end milling and drilling in terms of the continuous change in FOA encountered by the tool. Additionally, it has been noted (for instance, Wang and Zhang [3]) that the nominal and actual depths of cut are very different in planing-type cuts, due to the large elastic strain that can be accommodated by CFRP composites. Orthogonal cutting of disks can be carried out over multiple revolutions until the feed stabilizes at the required value.

Many finite element studies have been conducted to study the effect of FOA on these outputs, but they are all restricted to incipient cutting conditions, during which the thrust forces and temperature do not match values measured under steady state cutting conditions. Longer duration simulations such as those used for metal cutting are currently being developed. Data obtained in this study can be used to verify and calibrate these simulations.

BACKGROUND

The force required to cut through the fibers depends on the fiber orientation angle, edge radius, feed, etc. This dependence, and the resulting damage underneath the machined surface, need to be quantified in order to understand and model the impact of forces on different modes of damage. This can be carried out only by studies using unidirectional CFRP; in multi-directional laminates it is not possible to study the variation in force with respect to fiber angle.

There have been many studies of the machining of unidirectional fiber reinforced polymers (FRP). Koplev et al. [2] carried out a thorough study of the forces and damage occurring during orthogonal cutting of unidirectional CFRP in a planer. They used an adhesive layer on the free surface to obtain “macrochips” and found that chip formation was dominated by fracture with little

evidence of plastic deformation. They found that for a 90° FOA, only the matrix was visible on the machined surface, but cracks were found to extend 0.1 mm to 0.3 mm into the surface. For 0° FOA, they found cracks ahead of the cutting edge, but none extending into the machined surface. They found the cutting force to increase with depth of cut (which is also the feed for orthogonal cutting), and decrease slightly with rake angle. The thrust force was found to be independent of the above two variables, but it decreased dramatically as the relief angle increased. These observations were used to infer that the cutting force was related to chip making along the rake face and the thrust force was mainly due to the rubbing of the machined surface along the flank face. The cutting speed was not found to affect the forces appreciably. The cutting edge radius was not mentioned, but was likely smaller than the 0.05 mm minimum depth of cut used. The FOA used for the cutting force study was not reported. They also observed an increase in the thrust force within a few meters of cutting length, and attributed it to tool wear.

Wang, Ramulu, and Arola [4] carried out an extensive set of orthogonal cutting tests to study the effect of FOA and cutting conditions on chip formation and forces. They do not mention the cutting edge radius used, but it can be inferred from the results that it is small compared to the large values of depth of cut used (0.25 mm). They found that the thrust force was larger than the cutting force for positive FOA up to 75°, and attributed this as well as the decrease in thrust force beyond 60° to elastic recovery of cut fibers. They resolved the cutting forces into components normal to the fiber and along the fiber and found for one condition with a high clearance angle ($\gamma=17^\circ$) that the normal force remained constant for FOA between 15° and 75°. For 90° and higher FOA the cutting force increased dramatically, with jumps in the component of cutting force normal to the fiber direction as well as the direction of the resultant cutting force. They listed fracture along the fiber-matrix interface and fiber fracture by compression induced shear among the mechanisms.

Wang and Zhang [3] carried out planing-type cuts and found a different behavior of the cutting force vs. FOA at a very low depth of cut of 0.001 mm compared to that for 0.050 mm. In the former case, the cutting force increased with FOA to 60° and then decreased until 120°. For normal depths of cut, the cutting force increased with FOA to 120°, with the increase being especially steep for 90° and 120°. They also found that the actual depth of cut was smaller than the nominal depth of cut, and attributed this to elastic “bouncing back” of the material, arising from the bending of the fibers. It was surmised that this bouncing back would be related to the edge radius, but the edge radius of the tools used was not specified. They also found that, for small depths of cut, the fibers only bent but were not cut, and only the epoxy matrix was cut, resulting in fibers protruding out of the surface. This was attributed to the cutting edge radius causing a compressive stress along the fiber.

Many recent studies on the end milling of CFRP have focused on the key role of the cutting edge radius in producing machined surface with lower damage. Faraz et al. [5] quantified drill wear using cutting edge radius as the measured parameter and found that it correlated well with forces, damage, etc. Dold et al. [6] measured changes in the cutting edge radius of polycrystalline diamond (PCD) turning inserts to study whether laser machining of PCD inserts is a feasible technique for preparation of cutting edges. They found that the wear rate depended on the fiber angle, with the largest wear rate observed at 90° FOA. They found that in about 1.6 minutes of cutting at a material removal rate of 20 mm³/mm/min, the cutting edge radius increased to between 20 μm and 30 μm from a starting value of about 5 μm. Ishimaru et al. [7] recently developed a novel method of polishing PCD inserts that led to very sharp cutting edges (of edge radius 0.5 μm) and showed that this led to clean cutting of the fibers and matrix, at low forces, and with reduced surface damage as compared to cutting with a 5 μm edge radius tool.

Many finite element studies [1,8-11] have been carried out to understand the cutting mechanisms for different FOAs. 2D plane stress elements are typically used to model alternating lamellae of fibers and matrix, and damage models are used to model tensile failure in the fiber, plastic damage in the matrix, and mode I and mode II failure along the interface. These studies provide good insights into the likely mechanisms behind cutting force and damage generation. They all show that the interplay between the cutting edge radius, depth of cut, and FOA determines the mechanism of material removal.

While it is well recognized that the edge radius plays an important role in the forces and surface damage encountered in CFRP machining, only a limited number of experimental studies have been carried out on this topic. Delamination, fiber pull out, and other forms of damage depend on the interplay between cutting edge–fiber interactions (bending, crushing and fracture of fibers around the cutting edge), and fiber–matrix as well as interlaminar adhesion. There is a need for more experimental studies on the role of fiber diameter, cutting edge radius, depth of cut, and material properties in determining the relationship between FOA and cutting forces.

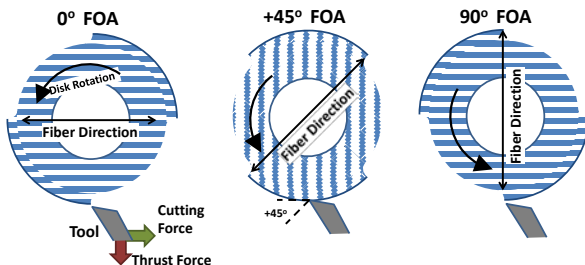


Figure 1 Schematic showing continuously changing fiber orientation angle (FOA) over one tab, over 1/4 revolution.

EXPERIMENT PROCEDURE

The workpiece disks are 6.4 mm thick and 133.4 mm diameter machined from unidirectional CFRP panels. The panels are made from stacked unidirectional pre-impregnated carbon fiber laminates. Some of the disks have woven single-layer outer plies to limit tearing of the outer unidirectional plies. Two slots are machined into the periphery of the disks which creates two tabs that are cut each revolution, as shown in Figure 1. The locations of the tabs with respect to the fiber direction are also shown in Figure 1. The tool cuts a continuously increasing FOA starting at 0° (fibers tangent to the disk surface and cutting velocity) and ending at 90° (fibers normal to the disk surface). In reality, the as-machined disks constitute a -5° to 95° transition. It is important to note that a positive FOA is as shown in the center image of Figure 1. For unidirectional laminates, negative FOAs can propagate cracks deep into the workpiece and cause separation along the fiber direction.

The tools are triangular inserts made of C5 commercial grade carbide with 30° rake and 10° clearance angles. Most tools are honed and have a straight or slightly rounded chamfer of width between 10 μm and 20 μm, except for Tests 24 and 25 which use the same “sharp” non-honed tool. The inserts are fixed in a custom tool holder which is mounted to a commercial 3-axis piezoelectric dynamometer aligned to measure the cutting force and thrust force. The machining is carried out in a high speed grinding center with tool and dynamometer mounted on a stationary B-axis, and CFRP disks are held in the spindle as shown in Figure 2. A laser displacement sensor is mounted between the spindle and tool slides to monitor the actual displacement in the feed (Y) direction. The tool is positioned in the cut (X) direction such that the edge is located directly below the spindle centerline. Three high speed cameras, two visible light and one infrared, are also mounted in the machining center, as shown in Figure 2.

The top visible camera is set to record a 512 pixel × 512 pixel region of interest (ROI) corresponding to a 7.8 mm × 7.8 mm field of view (FOV), and records at a frame rate of 800 frames per second (fps) for high speed tests and 100 fps for low speed tests (camera limit is 6 000 fps at this ROI). The top camera is focused on the disk surface before it reaches the cutting region. Shifting top camera video timing by the equivalent of one spindle revolution can provide ‘after cut’ or ‘before cut’ disk surface images (Figure 3). The bottom camera is set to a 512 pixel × 272 pixel ROI resulting in a 13.1 mm × 7 mm FOV and records at a frame rate of 7 000 fps for high speed tests and 1 000 fps for low speed tests (camera limit is 50 000 fps at this ROI). The bottom camera is positioned such that the viewing direction is between the cutting velocity and the normal to the rake face, and focused on the cutting region and tool rake face. Due to the high shutter speed, fiber-optic lights are used to illuminate the top and bottom camera viewing area. Before

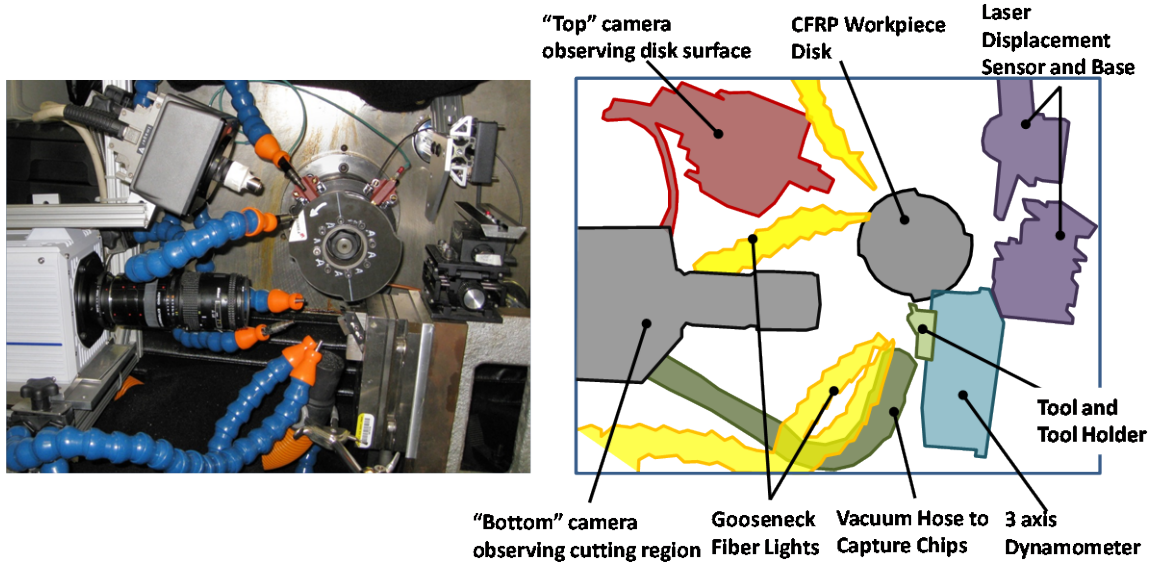


Figure 2 Machining setup in the high speed grinding center. The infrared camera is not shown, but observes the cutting region from the side along the cutting edge. The white line on the disk indicates the fiber direction.

each test, the shutter speed and gamma correction are set on each camera to obtain the best quality image.

The viewing direction of the infrared camera is along the cutting edge, perpendicular to the plane of the cutting process. A 50 mm lens is used with a 15 mm extension tube. The central quarter of the focal plane array is used to record a 160 pixel \times 128 pixel ROI, corresponding to a field of view of 6 mm \times 4.8 mm. The spectral sensitivity is set by a 3.786 μm to 4.056 μm bandpass optical filter. The integration time used is 240 μs , with variable frame rate up to 800 fps. The camera software uses a previously carried out blackbody calibration to convert pixel intensities recorded into equivalent blackbody temperatures (apparent temperature or radiometric temperature). The emissivity ϵ is

required to convert apparent temperature to true thermodynamic temperature. Since the chip/debris cloud is of constantly changing morphology and density, measuring the emissivity is a formidable task and has not been attempted here. Since $\epsilon < 1$, the apparent temperatures shown bound the lower limit of the true temperature.

Forces, laser displacement signal, spindle encoder signal, and camera timing signals are acquired with a digital oscilloscope at 1 MHz sampling rate. Forces are then down-sampled to 1 kHz, by averaging contiguous sets of 1000 data points, and the standard deviation of each set is used as a measure of the variation about the mean. An encoder output that goes from 0 to 1 during each revolution is generated during post processing by counting a 256

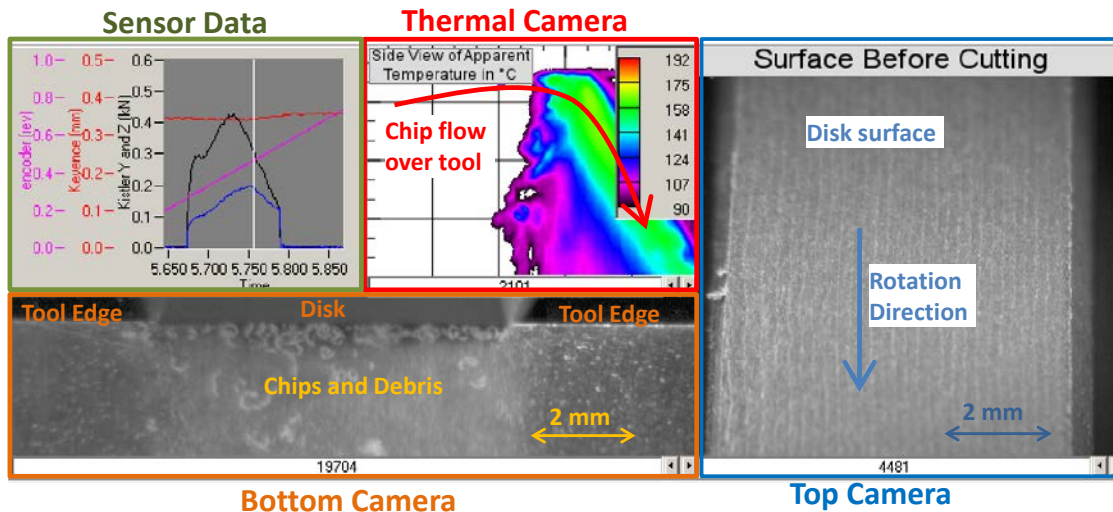


Figure 3 Example frame from a 'merged movie' showing the four sub-frames that constitute it, and annotations identifying the different components.

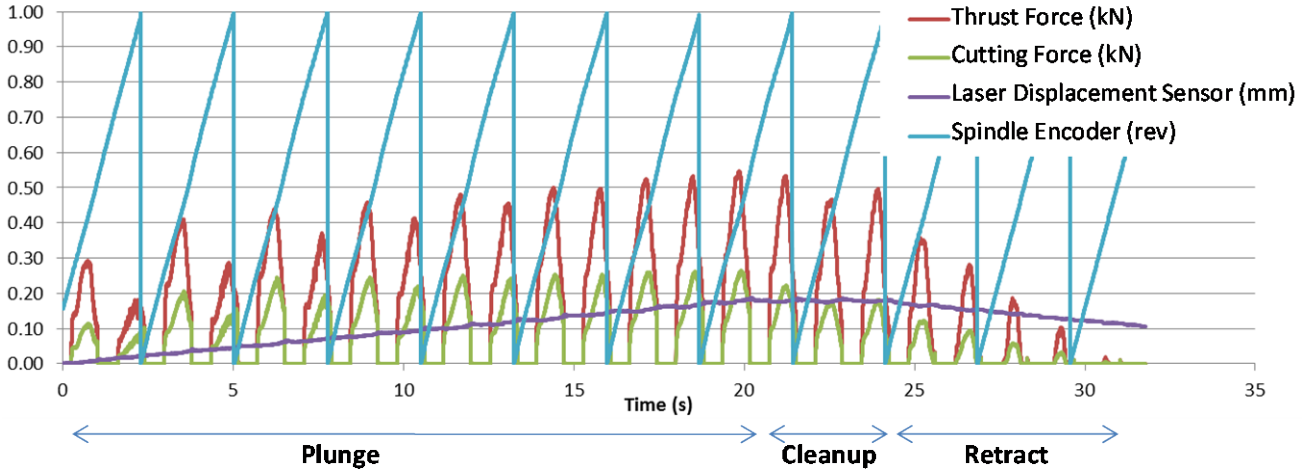


Figure 4 Example force and sensor test data for Test 8 (1.02 m/s, 0.025 mm/rev feed)

cycles/rev resolver signal, using a once-per-revolution proximity probe signal to set the zero. Synchronization of the three videos with sensor data is done in post-processing using custom software developed at NIST. The top camera image is moved to an earlier time corresponding to about 5/8 of a revolution to give a view of the machined surface (or advanced by about 3/8 of a revolution to give a view of the free surface of the workpiece) that is synchronized with the rake face view recorded by the bottom camera. Video frames are synchronized based on the bottom camera which records at higher frame rate. If a thermal or top camera frame occurs within a half frame of the bottom camera, then it is synchronized with that frame. For ease of analysis, camera video and sensor data are compiled into a ‘merged movie’ where frames from each camera are synchronized with the sensor data (see Figure 3) and incorporated as sub-frames that make up each frame of the merged movie. In the sensor data graph in the upper left corner, the thrust force (F_t , Kistler Y) is the black colored curve, the cutting force (F_c , Kistler Z) is the blue colored curve, and the time corresponding to the images is indicated by the vertical white line). An example screenshot of a merged movie is shown in Figure 3.

Table 1 gives the cutting conditions used for the cutting tests. The run-out of the as-fabricated CFRP disks may be larger than the 0.025 mm/rev feed depth. Therefore, initial truing or ‘cleanup’ cuts are made for each new disk at 0.025 mm/rev feed until the entire 6.4 mm width is seen to be cut in the bottom camera images. This was followed by a first cut at 0.025 mm/rev feed for a cutting distance of 1.52 m and a second cut at 0.127 mm feed for a cutting distance of 0.46 m. The longer cutting distance is used for the smaller feed to let the forces build up to steady state, which is affected by the elastic deflection of the disc. For Tool 6, two more tests (13 and 14) were carried out because the force data was not collected for Test 11 by mistake.

After the tests were completed, the tools and disk surface were observed under an optical microscope for wear and surface finish features. Tool cutting edges were also measured with a 3D profilometer to quantify tool wear at and around the cutting edge.

RESULTS

Tool forces and high speed video

An example of the sensor data collected during a test is given in Figure 4 for Test 8. As can be seen from the laser

Table 1 Summary of the experiments presented.

Test #	Speed (m/s)	Feed (mm/rev)	Woven outer ply?	Tool #	Tool condition before test	Cut dist. (m)
6	1.02	0.025	No	2	Honed, pre-cut 1.52 m.	0.46
7	1.02	0.127	No	2	Honed, pre-cut 1.98 m	0.46
8	0.15	0.025	Yes	5	Honed.	1.52
10	0.15	0.127	Yes	5	Honed. Pre-cut 1.98 m	0.46
12	0.15	0.127	No	6	Honed. Pre-cut 1.52 m	0.46
13	0.15	0.025	No	6	Honed. Pre-cut 2.82 m	1.52
14	0.15	0.127	No	6	Honed. Pre-cut 1.52 m	0.46
24	1.02	0.025	Yes	12	Sharp, pre-cut 1.52 m	1.52
25	1.02	0.127	Yes	12	Sharp, pre-cut 3.05 m	0.69

displacement sensor signal, the part program consisted of a ‘plunging’ phase in which the workpiece is fed into the tool at a constant rate, a ‘cleanup’ phase without any infeed for one revolution, and a ‘retract’ phase where the workpiece is lifted from the tool. Comparing the spindle encoder signal and the force data, it can be seen that there are two force “chirps” for each revolution, corresponding to the cutting of the two tabs. The cutting force tangential to the disk is smaller than the thrust force normal to the disk. The cutting force is about one-half of the thrust force during most of the cut, but at the beginning and end of engagement, it is even smaller. Due to the high elastic deflection of the CFRP material under the tool, it takes several revolutions of the disk before approximately steady-state cutting is reached. The cutting force chirps reach steady state at approximately

12 s in Figure 4, while the peak of the thrust force chirps seems to increase throughout the plunging phase. At near steady state, the force chirps corresponding to the two tabs are also nearly identical. The high elastic deflection is also evidenced by the forces measured during the ‘retract’ phase of the cutting cycle, with noticeable force chirps even after the tool has retracted 0.075 mm. Without elastic deflection, there should not have been any chirps beyond the end of the ‘cleanup’ phase.

To compare tests, exemplary force chirps were taken from the sensor data. These were selected towards the end of the ‘plunge’ phase in each test (e.g., the chirp between 18 s and 19 s was chosen for Test 8 in Figure 4). The chirps were plotted vs. encoder signal converted from revolutions to fiber angle. The starting fiber angle for each chirp is set to be -4° , determined by measurement of the tab locations with respect to the fiber direction. The exemplary force chirps for the four 0.15 m/s tests are shown in Figure 5, and exemplary force chirps for the four 1.02 m/s tests are shown in Figure 6. From these, the following trends can be noted (with the exception of Test 13): 1) Cutting tests with similar conditions incur similar force trends regardless of speed or outer ply, 2) the peak forces are slightly lower (up to 10 %) for the higher cutting speed, 3) the cutting force decreases after approximately 65° for low feed (0.025 mm/rev) tests, but continues to increase after 65° for high feed (0.127 mm/rev) tests, and 4) the peak cutting force is around one-half of the peak thrust force for the lower feed, but is about two-thirds of the peak thrust force for the higher feed.

Tests with similar cutting conditions showed similar force characteristics except for Test 13. Test 13 showed significantly higher magnitude of forces, as well as an egregious feature between 65° and 75° FOA. In addition, forces for Test 14 (with the same tool, disk, and conditions as Test 12, at 0.15 m/s, 0.127 mm/rev feed) were significantly higher than for Test 12. Tests 12, 13, and 14 were sequential cutting tests carried out with the same tool and disk, because by mistake force data was not collected for Test 11. The higher wear of the tool at the beginning of Test 13 is the likely reason for the forces in Test 13 being much higher than for Test 8.

In most cases, the peak cutting force occurs between 45° and 55° FOA for the 0.025 mm/rev feed, and close to 90° for the 0.127 mm/rev feed, once the actual feed after elastic deflections has ramped up to the steady state value. Peak thrust force consistently occurs between 45° to 55° FOA for both depths. Peak thrust force is 30 % to 40 % higher for the 5× higher feed. The peak cutting force is 90 % to 110 % higher for a 5× higher feed. This shows the peak cutting force is more sensitive to the change in feed (which is also the depth of cut), and becomes larger in comparison to the peak thrust force as the feed increases. However, these force-depth sensitivities are less than that observed by Koplev et al. [2], of 300 % to 350 % increase in cutting force and 300 % increase in thrust force for a 4× increase in

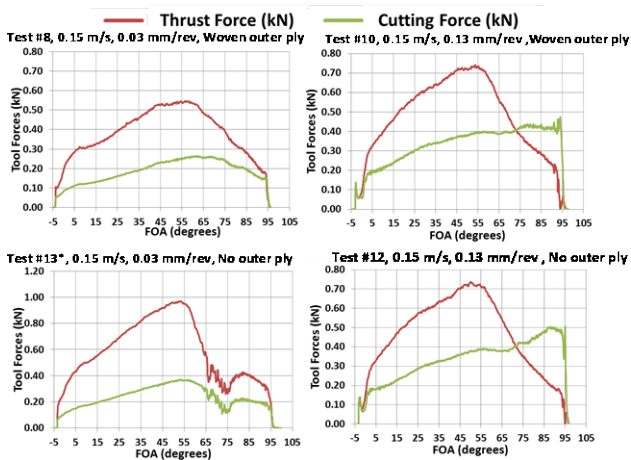


Figure 5 Exemplary force chirps for 0.15 m/s tests. Note that Test 13 data is on a different vertical scale and was performed after Test 12 at 0.127 mm/rev, which produced a different response when compared to Test 8 and Test 10 due to the additional tool wear experienced at the higher feed.

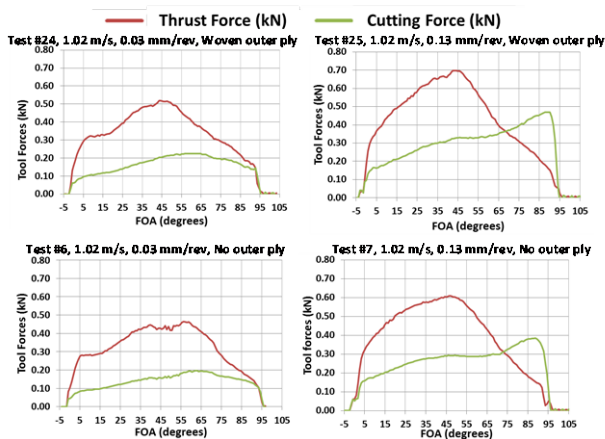


Figure 6 Exemplary force chirps for 1.02 m/s speed tests.

feed.

All merged movies were observed and trends in chip formation noted. For this study, only qualitative trends were noted from videos. Attention was given to the post 60° FOA portion of cutting in the merged movies where forces for the high and low feed tests differ the most. Figure 7 shows example merged movie frames for tests of similar cutting conditions. From the sensor data graphs, it can be verified that the images correspond to about 80° FOA.

A clearly apparent difference in the 60°+ FOA region is that higher feed cuts showing increasing cutting force produced continuous chips whereas low feed cuts showed broken dust and debris. At low cutting speed, the continuous chip curled away from the tool and blocked the bottom camera view, but was visible in the thermal image as seen in Figure 7c. At the higher speed, the chip appeared continuous in the bottom camera view, and flowed close to the rake face as in Figure 7d.

Similar to Wang et al. [4], forces normal and tangential (shear) to the fiber direction (Figure 8) were calculated from the cutting and thrust force components using equation 1.

$$\begin{aligned} N_s &= F_c \sin \theta + F_t \cos \theta \\ F_s &= F_c \cos \theta - F_t \sin \theta \end{aligned} \quad (1)$$

The shear force (F_s) becomes negative around 30° and reaches a minimum around 50°, similar to Wang et al.'s results. The calculated normal force (N_s) has a local maximum around 35° to 45° FOA. These results compare well with the earlier data, which shows that turning a continually varying FOA disk is a valid method for studying FOA effects in CFRP cutting. However, the trends in forces around the 0° and 90° FOAs are different from those reported earlier, and are found to vary significantly depending on the actual amount of material cut during each force chirp. The difference may also be partly attributable to end effects at the beginning and end of each cut of the tabs, which coincide with 0° and 90° FOA, respectively.

Microscopy and profilometry of inserts used

Since the cutting edge radius is an important determinant of cutting forces and damage, inserts used for the tests were observed under an optical microscope and characterized under a 3D profilometer.

Optical microscopy led to several interesting observations. When the rake face of the inserts used was observed under brightfield illumination, some debris could be observed outside the contact area between the chip and the rake face. A faint impression of abrasion of the rake face by the fibers, localized to a small region adjacent to the cutting edge, could also be discerned. Comparing the region of the rake face in the cut with that outside (to the left of the arrow in Figure 9), it was also noted that the cutting edge was found to have migrated inwards from its original location in the cutting region, likely due to flank wear. This

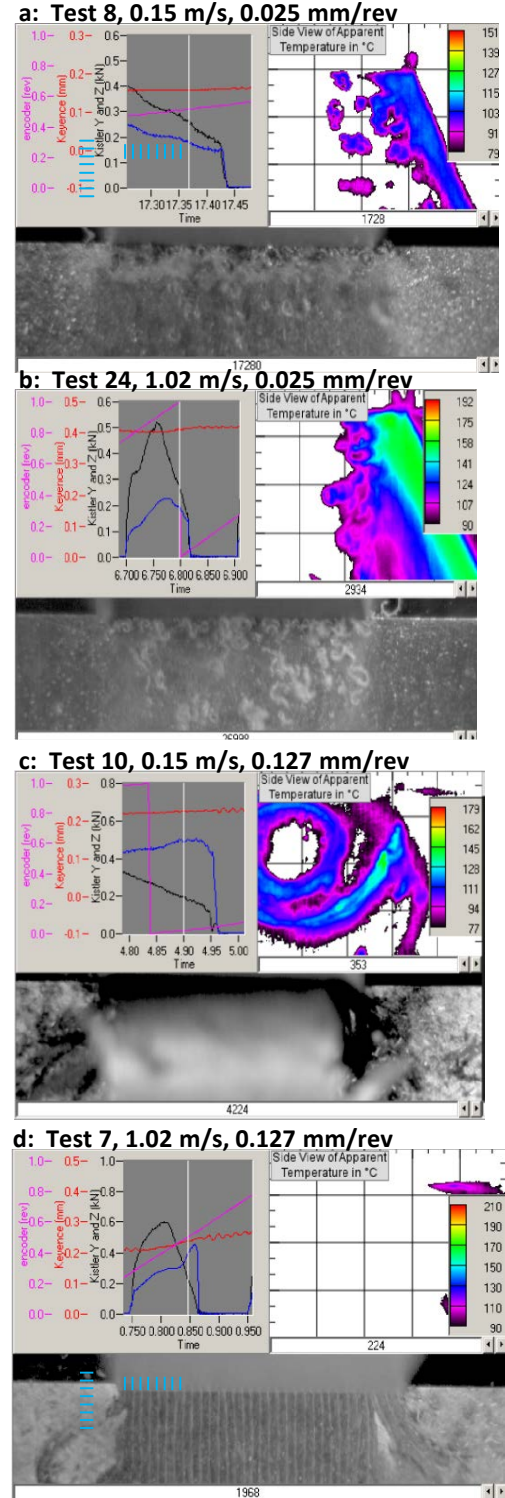


Figure 7 Example merged movie frames acquired at about 80° FOA. a) Discontinuous, small fibers and debris hug the rake face. b) Discontinuous, small fibers and debris hug the rake face. c) Large, tightly curled continuous chip. d) Continuous chip with minimal breakage and chips hug the rake face.

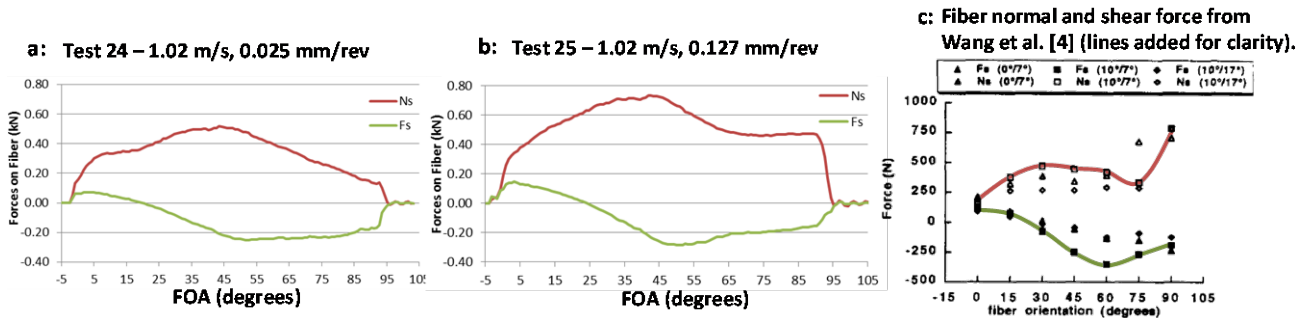


Figure 8 Tangential (F_s) and normal (N_s) forces, parallel and perpendicular to the fiber direction, for high speed (1.02 m/s) tests. a) Example calculation for low feed (0.025 mm/rev). b) Example for high feed (0.127 mm/rev) c) Visual comparison with results from Wang et al. [4].

was found to be the case for all four of the inserts used for the tests discussed here.

Figure 10 shows the flank faces of two of the inserts used. In the low magnification image of Tool 6 in Figure 10(a), it is clearer that the cutting edge has receded into the insert due to erosion. Another interesting observation is the periodic grooving of the cutting edge, with a uniform spacing that matches the ply thickness of the work pieces. This erosion pattern can be attributed to the higher fiber fraction within plies as compared to the interlaminar region within which the fiber fraction is smaller. The higher hardness and stiffness of the fibers cause fiber rich regions to abrade more the region of the cutting edge they engage with. The observed grooving along the flank face is strong evidence that the flank wear is entirely due to abrasion by the cut fibers that travel under the cutting edge, along the machined surface.

Figure 10(b) shows a magnified image of the flank face of Tool 12 (a nominally sharp tool for which the cutting edge was not honed), in the middle of the cutting edge region engaged in cutting. A flat region of flank wear can be observed wherein the inclined pattern of grinding grooves on the rest of the flank face is replaced with an erosion pattern perpendicular to the cutting edge, along the direction of sliding of the cut fibers on the machined surface. The flank wear width is about 95 μm . The periodic pattern is visible in this image also, although it is not as pronounced as for Tool 6.

Figure 11 shows a brightfield illumination image of the cutting edge of Tool 6 as viewed from the cutting velocity direction, with the field of view covering the left end of the extent of the cutting edge that is engaged in cutting the workpiece. To the left of the arrow, the unused portion of the honed cutting edge appears uniform and straight. In contrast, the used portion of the cutting edge is seen to undulate on account of the periodic wear pattern of the cutting edge. The periodic pattern is more pronounced in the middle of the cutting edge (not shown here) as can be noted from Figure 10(a). It is also interesting that the reflection from the worn region of the cutting edge is

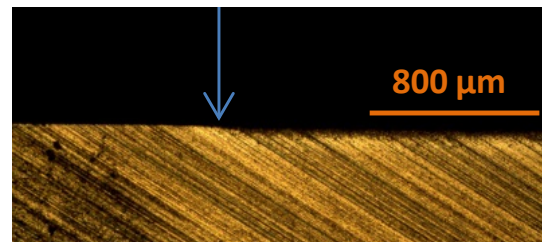


Figure 9 Optical microscope image of the rake face of Tool 5, showing the left end of the contact between the rake face and the chip. The cutting edge to the right of the arrow was engaged in cutting and can be seen to have slightly receded into the body of the insert.

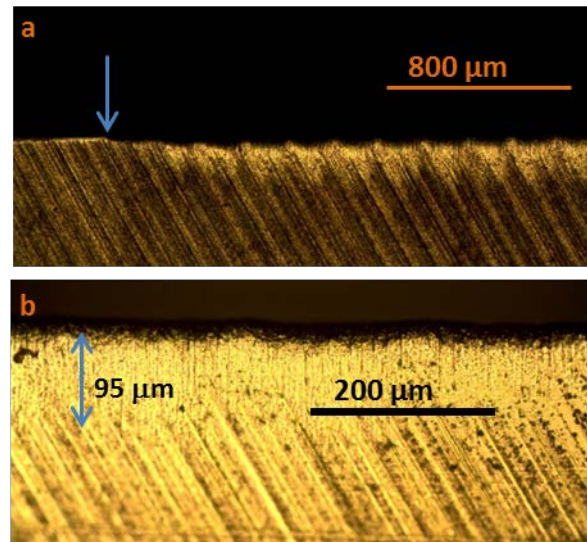


Figure 10 (a) Low magnification view of the flank face of Tool 6 showing recession and periodic grooving of the edge to the right of the arrow that is engaged in cutting. (b) Higher magnification image of the flank face of initially sharp Tool 12 showing the development of a 95 μm wide flank wear land.

narrower than that from the unused region of the edge prepared by honing. Since the incident light and the imaged reflected light are both in the direction of view for brightfield illumination, the narrower reflection can be inferred to indicate a sharper edge.

Figure 12(a) shows a 3D profile of the cutting edge of Tool 6, over the middle of the region engaged in cutting. This was measured by white light interferometry, using a 50× objective, with a 210 μm × 210 μm field of view. The worn region of the flank face is at the top. The lower portion of the 3D profile does not quite extend into the rake



Figure 11 Brightfield illumination image of the cutting edge as viewed along the cutting direction. The region to the right of the arrow is engaged in cutting the workpiece and can be seen to have been grooved and to have receded into the insert.

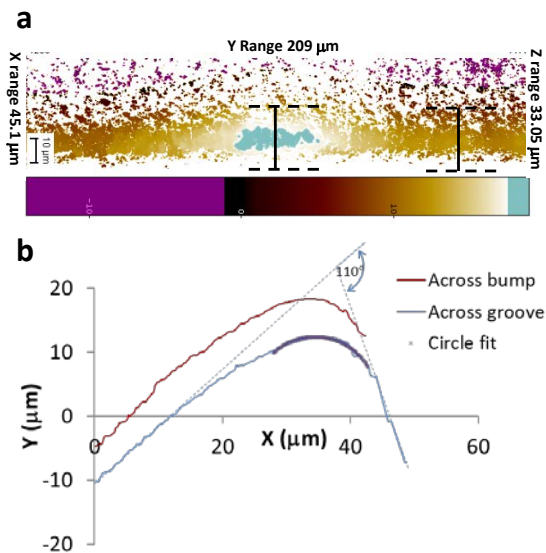


Figure 12 (a) Plan view of 3D profile of the cutting edge of Tool 6, with colors representing the heights, showing a bump in the middle flanked by two grooves at left and right. (b) 2D profiles across the cutting edge, taken over the bump and the groove on the right, at the locations shown in (a). The extent of the region over which these profiles are averaged is shown by the width of the 'I'.

face, but is nearly at the end of the cutting edge and the beginning of the rake face.

The locations of two profiles across the cutting edge, one over a groove and the other over a bump in between the two grooves, are shown in Figure 12(a) and the two profiles are shown in Figure 12(b). The profiles are quite similar to one another. The total change in angle of the local tangent to the curve over the measured region is 110° as shown in Figure 12(b). The change in angle of the tangents, between the wear flat on the flank face and the rake face, is expected to be 120°, since the rake angle is 30° and the wear flat is assumed to be parallel to the machined surface. When the scanning depth during measurement of the 3D profiles is increased, the measured angle change approaches 120° for worn regions and 130° for unworn regions.

The best fit circle to the cutting edge, also shown in Figure 12(b), had a radius of about 10 μm for both profiles, and the radius is quite insensitive to the extent around the cutting edge chosen for fitting. As mentioned before, the edge prepared by honing could either be characterized as a chamfer of width 10 μm to 20 μm, or could be approximated as a circular segment of radius between 15 μm and 20 μm. This shows quantitatively that, for this type of edge prep, the cutting edge is actually becoming sharper in the worn region. The difference in the X- and Y-coordinates of the center of the circle fit to the edges in the two profiles are 1.6 μm and 5.6 μm, respectively. These values are affected a bit by how well the cutting edge has been aligned along the Z- axis, but still are a good measure of the relative depth of the grooves (with respect to the bumps) in the rake and flank faces, respectively.

Figure 13(a) shows a 3D view of the 3D profile data in Figure 12, the viewing direction being such that the flank face is in the foreground. The grooving is clearly apparent. A profile along the cutting edge, at the top of the ridge, is shown in Figure 13(b), from which it can be seen that the depth of the grooving is about 6 μm on one side and 8 μm on the other. It can also be noted that the pitch of the grooves, from trough to trough on the profile in Figure 13(b), is about 170 μm.

Figure 14(a) shows a 3D profile of the flank face of Tool 6, over the middle of the region engaged in cutting, with the cutting edge on the right side. The extent of flank wear can be estimated based on the visibility of the grinding grooves over the unworn portion of the flank face, on the left side. Periodic grooving of the cutting edge, due to extra abrasion by the fibers in the plies, is again evident. While flank wear is less behind the bumps and more behind the grooves, the minimum flank wear is about 85 μm and the average flank wear is about 110 μm. Figure 14(b) shows a 3D view of the flank face surface showing a groove in the middle of two bumps caused by the fibers. For the sake of clarity, heights along the Z- axis are magnified 3× and gaps in the data have been filled.

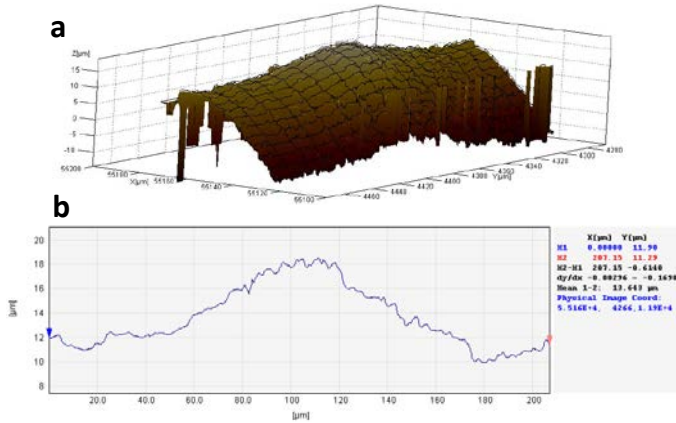


Figure 13 (a) 3D view of the 3D profile of the cutting edge, showing a bump between two grooves caused by the extra abrasion of the fibers in the plies. (b) Line profile along the top of the cutting edge showing that the local groove depth is about 8 micrometers.

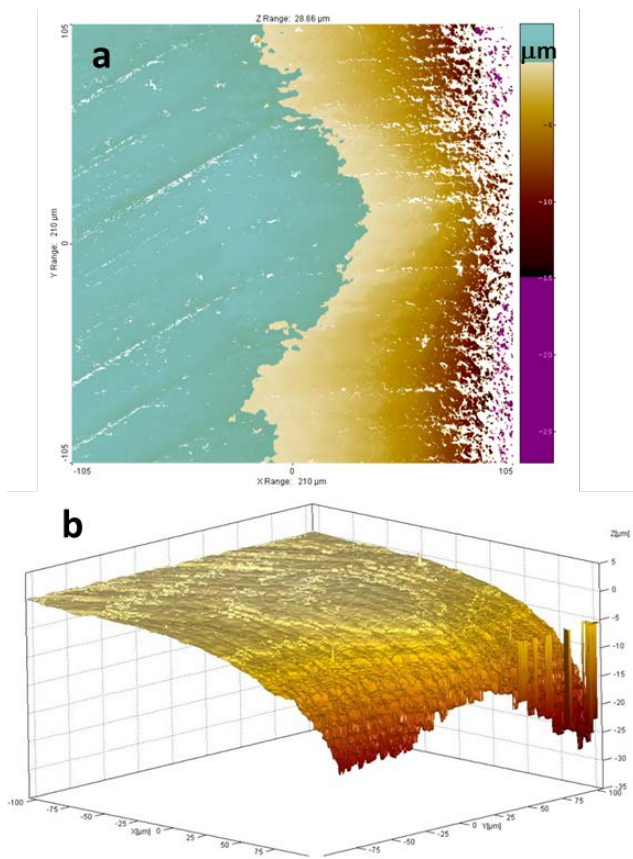


Figure 14 3D profile of the flank face of Tool 6 with the cutting edge on the right side. (a) Plan view with colored fringes showing periodic grooving of the cutting edge as well as grinding grooves visible over the unworn portion of the flank face. (b) 3D view of the flank face (heights along the Z-axis are magnified 3x and gaps in the data have been filled).

DISCUSSION

As reported extensively in the literature ([2-4], for instance), it is observed that the thrust force is higher than the cutting force for FOAs less than 60°. It continues to remain smaller until 90° for the smaller feed of 0.025 mm/rev, while for the larger feed of 0.127 mm/rev, the cutting force typically becomes larger than the thrust force at some angle between 65° and 75°.

Both the microscopic images and the 3D profiles show that there is significant flank wear and grooving of the tools, even within the short duration used for the cutting experiments. The grooves indicate that the cut fibers are quite abrasive and able to erode the carbide tool material rapidly from the flank face of the cutting tool. The high flank wear, along with the high positive rake angle of 30° causes the cutting edge to recede into the insert.

Due to the large starting edge radius of the honed inserts, the worn cutting edge appears sharper in microscopic images (Figure 11). Profiles across unworn regions of the cutting edge showed that the edge prepared by honing could either be characterized as a chamfer of width between 10 μm and 20 μm, or could be approximated by a circular segment of radius 15 μm to 20 μm. In comparison, worn regions of the cutting edge had radii close to 10 μm.

An estimate of the progressive wear of the cutting edge with cutting time was obtained by comparing profiles of the edge near the ends of its engagement with the workpiece width (i.e., in regions engaged in cutting the outer plies) with those along the middle of the engagement width, as shown in Figure 15. The profiles shown from top to bottom in Figure 15(b) are in the order of increasing wear. The top profile is that of an unworn portion of the edge just outside the engagement width, which can be approximated as a 15 μm wide chamfer at a negative rake angle of about 15°. With wear, the cutting edge progressively moves into the insert. It can be seen from Figure 15(b) that the flank face of the tool undergoes the most wear, due to erosion by the highly abrasive cut fibers on the machined surface.

The left most portion of each profile represents the region of the cutting edge that is responsible for cutting the fibers. The radius of curvature of a circle fit to this 'operative region' is found to decrease for the profiles from top to bottom, i.e., with increasing wear the edge radius of the operative region of the tip decreases. This indicates that abrasive wear along the flank surface (caused by cut fibers rubbing along it) is dominant compared to the wear of the cutting edge expected from cutting the fibers. Abrasive wear of the flank face by the cut fibers causes an effect on the edge that is similar to the way chisel edges are sharpened by lapping one face on a whetstone. The "stiffness" of the mechanical means that causes the wear will determine the naturally resulting radius of the edge, in a manner similar to a hard lapping plate producing a sharper edge as compared to a soft polishing pad. The above

analogy suggests that the edge radius that naturally results due to wear will be determined by a few factors such as fiber diameter, bundle size, fiber adhesion to the matrix material, workpiece compliance, etc. Whether a cutting edge is initially prepared to a diameter greater than or smaller than this radius, the worn edge will assume its natural wearing radius. For the particular experimental conditions here, the natural wearing radius of the edge seems to be around 10 μm .

Figure 16 compares forces for tests 12 and 14, repeated with tool 6 under the same speed of 0.15 m/s and feed of 0.127 mm/rev. The thrust and cutting forces are observed to increase significantly with wear for FOA < 60°. The peak thrust force, increases $\approx 50\%$ (370 N), while the peak cutting force increases $\approx 25\%$ (100 N).

For FOA > 60°, the forces do not change significantly, but vary cyclically across chirps. For chirps where the forces for this FOA range in test 14 are larger than those in test 12, the increase in cutting force is actually larger than the increase in thrust force. It should be noted that, for the 30° rake angle of the tool, at 60° FOA the fibers are perpendicular to the rake face. Given a fairly sharp operative region, the relative slip between the cutting edge and the fiber, that occurs until the edge is able to break through a bundle of fibers, changes direction for FOA greater than the rake angle. This causes the cutting component of thrust force to reverse direction, striving to pull the tool into the workpiece. For this reason, for FOA > 60°, increase in the cutting component of the force would act to decrease the total thrust force, serving to offset part of the increase in thrust force due to wear. This is also the

reason chirps with very large cutting force near 90° FOA show very low or negative thrust force.

If most of the increase in cutting and thrust forces in test 14 over those in test 12 (for FOA < 60°) were to be attributed to increase in rubbing contact along the flank wear region, the coefficient of friction at this contact can be inferred to be $\approx 0.27 (=100/370)$. Furthermore, assuming that most of the thrust force is generated at the rubbing contact along the flank, it can be inferred that ≈ 200 N and ≈ 300 N of the peak cutting force are spent overcoming friction in tests 12 and 14, respectively, and about 200N is spent in the cutting action (i.e., in breaking fiber bundles and causing mode 2 fracture of the matrix along the FOA to propagate the crack to the free surface and remove a chunk of material, as described by Arola et al. [11]).

Figure 16 also shows forces for test 13 carried out in between tests 12 and 14, but at a fifth of the feed (0.025 mm/rev). For FOA < 60° the thrust force for test 13 is in between those for tests 12 and 14, but the cutting force is smaller than that for test 12. For FOA > 65°, the forces in test 13 are lower than the peak cutting forces observed in tests 12 and 14, but sometimes higher than the forces observed in tests 12 and 14 when cutting a pitted surface. The peak friction force along the flank face for test 13 is estimated to be 230 N (corresponding to the peak thrust force of 850 N), implying that ≈ 100 N is expended in the cutting action. The assumption that all of the thrust force originates at the flank face contact is the likely reason why the cutting component of force does not scale in proportion to the feed per revolution. An improved model of the cutting action of the fibers, that includes the bending

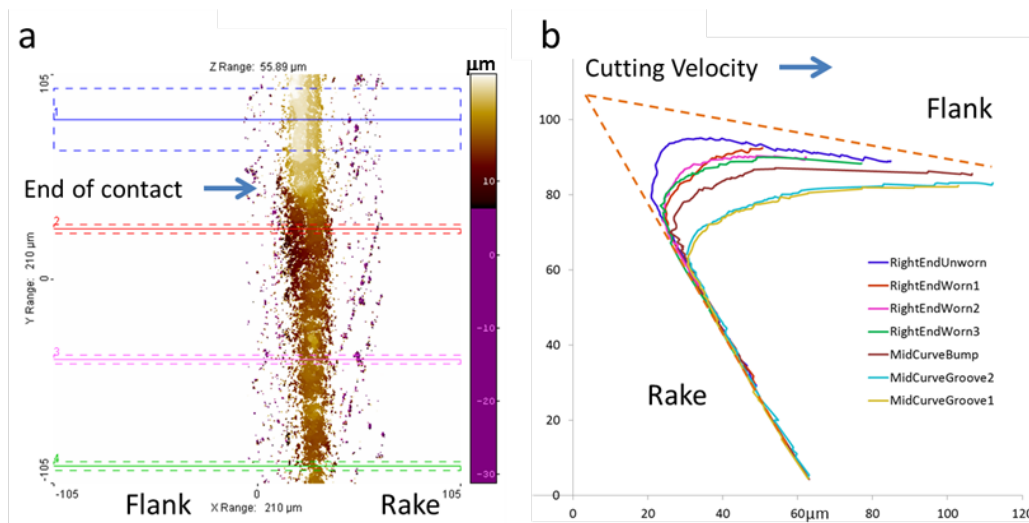


Figure 15 (a) Plan view of a 3D profile of one end of engagement of the cutting edge with the workpiece, with colored fringes representing Z-heights. Solid lines indicate the direction along which profiles are taken and hidden lines indicate the extent over which lines parallel to the solid line are averaged. (b) Profiles across the cutting edge taken at unworn and worn regions. The colors match the color of the solid line in the 3D plan view image. The orange ‘dashed’ lines estimate the boundaries of a perfectly sharp tool with 30° rake and 10° flank angle, enveloping all the profiles. These are used to position the three other profiles of the cutting edge at the middle of its engagement with the workpiece that are also shown in (b).

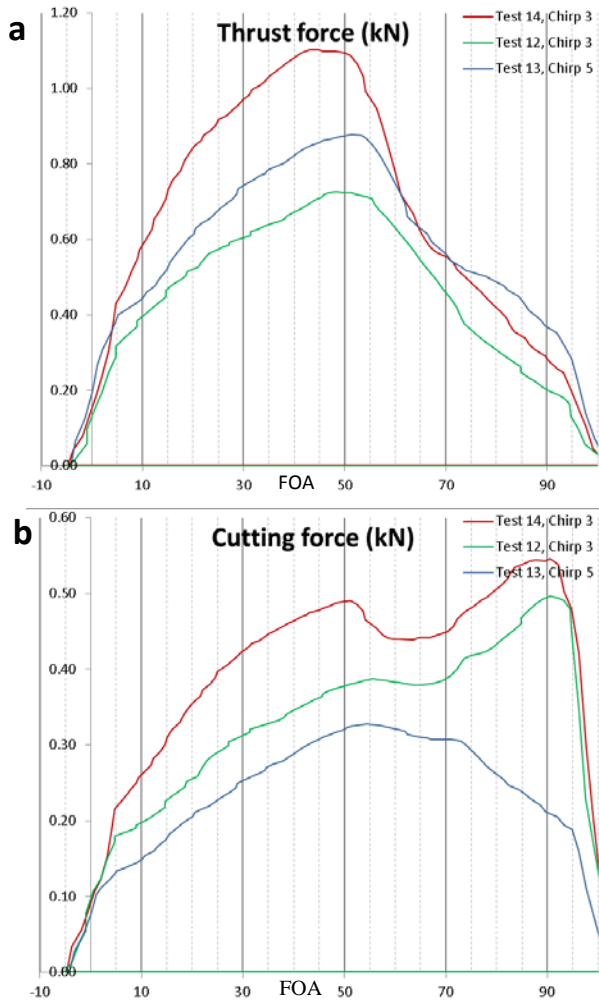


Figure 16 Comparison of the peak (a) thrust and (b) cutting force chirps encountered on one tab during consecutive tests 12, 13 and 14, with the same tool and workpiece disk. It can be seen that the thrust force in (a) increases with tool wear and is insensitive to the fact that test 13 is at 0.025 mm/rev feed as compared to 0.127 mm/rev for tests 12 and 14. The cutting force is sensitive to feed, and is quite different for low and high cutting feeds for FOA > 65°.

contribution to the maximum tension along the fiber direction, may be able to explain the observed force trends better.

The observed increase in thrust force with tool wear can be used to develop a model for the thrust force, based on the stiffness of the workpiece disk and the width of the disk. This can be coupled with a model for the force required at the cutting edge to fracture the fibers in tension and shear the matrix to propagate the strain to the free surface, to develop a complete force model for the process taking tool wear into consideration.

If the flank angle were higher, then the rate of rise in cutting forces and machined surface damage would be expected to be smaller. Based on contact mechanics, the contact pressure is constant for a given elastic deflection of the surface, independent of flank wear or flank angle. The wear rate normal to the flank wear land can be assumed to be proportional to the contact pressure and the number of fibers abrading the flank face, and since these do not change with flank angle, it is likely that the rate of recession of the edge into the insert will not increase. This suggests that increasing the flank angle to a higher value may be a way to reduce cutting forces and damage, without any added penalty in terms of tool life or higher geometric error.

CONCLUSIONS

Orthogonal cutting of disks of unidirectional CFRP laminates has been used to study the influence of fiber orientation angle and cutting condition on forces and chip formation. This has been shown to be a valid method to study the effect of a continuum of FOAs between 0° and 90°. As observed in earlier investigations, the cutting force increases with FOA until an angle of 90° for larger feed, but decreases beyond 65° for smaller feed. For FOA > 65°, continuous chips are associated with chirps showing an increase in cutting force, while powdery chips are observed for chirps showing a decrease in cutting force.

It has been found that tool wear rate of the carbide cutting tool is very high. Flank wear is the dominant mode of wear, and the mechanism is abrasion/erosion by the hard and abrasive carbon fibers. This causes the cutting and thrust force to increase significantly for FOA < 60°. Interestingly, it is found that the radius of the operative region of the cutting edge decreases due to the high value of the initial edge hone radius. For FOA > 65°, wherein the fibers mostly engage with the operative region of the cutting edge, there is no systematic change in cutting forces with wear. Cyclic variations in force signal are observed over this region. For this FOA region, chirps showing a small spike in the cutting force cause pitting of the machined surface, and lead to reduced forces in subsequent force chirps.

For CFRP cutting studies with carbide tools, the cutting length needs to be kept the same for different cutting conditions, for comparative study of the effect of different cutting parameters without the confounding effects of tool wear. Alternately a tool material such as PCD that exhibits much smaller wear rate should be used if the intention is solely to study mechanisms generating cutting force and machined surface damage.

ACKNOWLEDGMENTS

We thank Alkan Donmez for facilitating the research partnership. We are pleased to acknowledge the gracious loan of the infrared camera by the Materials Measurements Group at NIST (Steve Mates). We thank Alkan Donmez, Shawn Moylan, and Kevin Jurrens of NIST for thorough reviews of the manuscript.

REFERENCES CITED

- [1] Rentsch, R., 2012. Crack formation and crack path in CFRP machining, Proceedings of Crack Paths (CP 2012), Gaeta, Italy 2012.
- [2] Koplev, A., Lystrup, A., & Vorm, T. (1983). The cutting process, chips, and cutting forces in machining CFRP. *Composites*, 14(4), 371-376.
- [3] Wang, X. M., & Zhang, L. C. (2003). An experimental investigation into the orthogonal cutting of unidirectional fibre reinforced plastics. *International Journal of Machine Tools and Manufacture*, 43(10), 1015-1022.
- [4] Wang, D. H., Ramulu, M., & Arola, D. (1995). Orthogonal cutting mechanisms of graphite/epoxy composite. Part I: unidirectional laminate. *International Journal of Machine Tools and Manufacture*, 35(12), 1623-1638.
- [5] Faraz, A., Biermann, D., & Weinert, K. (2009). Cutting edge rounding: An innovative tool wear criterion in drilling CFRP composite laminates. *International Journal of Machine Tools and Manufacture*, 49(15), 1185-1196.
- [6] Dold, C., Henerichs, M., Bochmann, L., & Wegener, K. (2012). Comparison of ground and laser machined polycrystalline diamond (PCD) tools in cutting carbon fiber reinforced plastics (CFRP) for aircraft structures. *Procedia CIRP*, 1, 178-183.
- [7] Ishimaru, D., Tougea, M., Mutaa, H., Kubota, A., Sakamoto, T., & Sakamoto, S. (2012). Burr suppression using sharpened PCD cutting edge by ultraviolet-ray irradiation assisted polishing. *Procedia CIRP*, 1, 184-189.
- [8] Venu Gopala Rao, G., Mahajan, P., & Bhatnagar, N. (2007). Machining of UD-GFRP composites chip formation mechanism. *Composites science and technology*, 67(11), 2271-2281.
- [9] Dandekar, C., & Shin, Y.C. (2008). Multiphase Finite Element Modeling of Machining Unidirectional Composites- Prediction of Debonding and Fiber Damage. *J. Mfg. Sci. & Eng.*, 130, 051016-1 – 051016-12.
- [10] Calzada, K. A., Kapoor, S. G., DeVor, R. E., Samuel, J., & Srivastava, A. K. (2012). Modeling and interpretation of fiber orientation-based failure mechanisms in machining of carbon fiber-reinforced polymer composites. *Journal of Manufacturing Processes*, 14(2), 141-149.
- [11] Arola, D., Sultan, M.B., & Ramulu, M. (2002). Finite element modeling of edge trimming fiber reinforced plastics. *Journal of Manufacturing Science and Engineering*, 124, 32-41.